Performance evolution and tensile behaviour of long-term exposed UHPC under sustained load, aggressive environments and autogenous healing

Marco Davolio[1*], *Giovanni* Recchia[1], *Maria Ylenia* Altomare[1], *Francesco* Soave[1], *Salam* Al-Obaidi[1,2], and *Liberato* Ferrara[1]

[1]Politecnico di Milano, Department of Civil and Environmental Engineering, Piazza Leonardo da Vinci 32, 20133, Milan, Italy
[2]University of Al-Qadisiyah, Roads and Transportations Engineering Department, Diwaniyah, Iraq

Abstract. An extended experimental campaign was conducted to analyse the evolution of UHPC tensile performance over time as affected by sustained flexural load and aggressive environments both interacting with its autogenous self-healing capacity. A new methodology including both destructive and non-destructive tests was proposed. Three different mix designs were tested, with steel fibres, crystalline admixture, and various nanomaterials. Specifically, the first batch included alumina nano-fibres, while the second one cellulose nanocrystals. The last one was used as a reference and did not include nanomaterials. Thin beam specimens (500x100x30 mm) were pre-cracked and exposed to three different environments, under four-point bending sustained load. The specimens were cured for 1, 2, 3, 6, 9, and 12 months respectively, being exposed to a chloride solution, geothermal water, and tap water as a reference. After the aforesaid scheduled exposure times, two nominally identical specimens were tested for each condition, the first in four-point bending and the second in direct tension. To compare the results, a simplified five-point inverse analysis was adapted for beams with different slenderness, providing a quadrilinear constitutive law derived from the structural flexural behaviour of four-point bending tests. Test results allowed to highlight the effects of each parameter – type of material and exposure – on the self-healing effectiveness and the tensile response, also defining their evolution over time. The self-healing process resulted in an almost complete recovery after the first two or three months, and the materials were able to maintain a constant performance over longer periods, regardless of the conditions they were exposed to.

1 Introduction

The demand for strategic infrastructures such as chemical plants and energy harvesting sites is constantly increasing. These structures are frequently subject to aggressive environments that compromise the durability of the structural elements [1,2]. Two of the main degradation mechanisms that can occur in concrete structures are corrosion of the reinforcement and leaching of the cementitious matrix. Concerning the former, since concrete is not able to withstand tensile stresses, cracks might appear in any structure subjected to any combination of axial, flexural, and shear/torsion actions. Thus, aggressive agents can freely penetrate inside the matrix and corrode the steel reinforcement once they have reached it and have accumulated at a sufficient concentration. Leaching, instead, is defined as the separation of Ca^{2+} ions from the cement paste and their release in aqueous solution. Both phenomena impair the durability of concrete structures. Currently available standards prescribe design specifications to delay the penetration of aggressive agents, requiring a minimum concrete cover, a minimum cement content, and a maximum water/cement ratio, together with a minimum characteristic compressive strength, according to the type of exposure. The cover acts as a passive layer, with negligible contribution to the mechanical response of the element cross-section. As a matter of fact, besides being merely prescriptive, this approach demands frequent maintenance, which significantly increases the operative costs of the structure [3–5]. The growing interest in alternative solutions led to the development of new cementitious materials [6]. One of the most promising solutions is Ultra-High Performance Concrete (UHPC). This category of cementitious composite features remarkable compressive strength [7] and likewise significant tensile strength, toughness, and ductility [8], owing to the presence of fibres. The H2020 European Project ReSHEALience aimed at developing a peculiar UHPC with enhanced durability properties in the cracked state [9]. In this framework, together with the development of the material, the project paved the way for a different structural design approach, tackling durability as a performance-based design target [10]. The peculiar characteristics of UHPC allowed, on the one hand, to reduce the area of concrete required in the section, owing to its remarkable compressive strength and the no longer negligible contribution of the tensile stress-bearing capacity. On the other hand, exploiting the

* Corresponding author: marco.davolio@polimi.it

aforesaid tensile performance of UHPC is a valuable alternative to steel rebars. This paradigmatic shift is strictly related to the capacity of the material to maintain its tensile performance along the service life of the structure. Consequently, studies regarding the long-term performance of UHPC in real structural serviceability scenarios are necessary. Furthermore, UHPC is characterized by a high cement content and a low water-to-binder ratio. Consequently, it has significant autogenous self-healing capability which can enable structures made of UHPC to achieve an even longer service life. The synergic action of the aforementioned characteristics of this material must be validated through monitoring at different scales, according to the performance-based approach proposed by the standards. In the framework of the H2020 ReSHEALience project, a basin to collect geothermal water was designed and built in a geothermal power plant in Chiusdino (Italy) [11,12], exploiting the previously described features of UHPC. The present work reproduced the service life conditions of the structure at mesoscale (i.e., lab-scale) level, and investigated the evolution of flexural and tensile response over time, addressing the contribution of self-healing to compensate initial cracking of the structure.

2 Materials

The UHPC investigated in the experimental campaign was specifically developed in the framework of the H2020 ReSHEALience project [13,14]. The concrete mix (Table 1) is characterised by a Portland cement (CEM I 52.5 R) combined with slag, a water-to-binder ratio of 0.18, short straight steel fibres (1.5%), sand as aggregate, and a superplasticiser. Additionally, a crystalline admixture (CA-Penetron Admix®) was provided to promote the autogenous self-healing capacity [15]. Since this material features higher durability compared to other UHPC mixes, it was also defined, in the framework of the project, as Ultra-High Durability Concrete (UHDC). To further enhance the mechanical and self-healing performances of UHDC, nano-constituents – alumina nano-fibres (ANF) and cellulose nanocrystals (CNC) – were respectively added to two different batches [16]. A third batch without nanomaterials was used as a reference.

Table 1. Components of the three mixes.

Constituents [kg/m^3]	CA-REF	CA+ANF	CA+CNC
CEM I 52.5 R	600	600	600
Slag	500	500	500
Water	200	200	200
Steel fibres	120	120	120
Sand (Ø ≤ 2mm)	982	982	982
Superplasticiser	33	33	33
Crystalline admixture	4.8	4.8	4.8
Alumina nano-fibres*	–	0.25	–
Cellulose nanocrystals*	–	–	0.15
*% by weight of cement			

3 Experimental campaign

The present work aimed at investigating the behaviour of 500x100x30 mm^3 UHPC thin beams obtained by cutting large and equally thick slabs cast on-site, and, thus, affected by any issue related to the production of real manufactures (including, e.g., thickness tolerance and fibres distribution). To reproduce service life conditions on the beams, a mechanical loading and different environmental exposures were applied to the specimens over different periods. The sustained load was applied to the specimens with a tailored steel frame, simulating a 4-point bending scheme. A detailed description of the setup is provided in [17] and is schematically shown in Figure 1. Three different exposures were used for the curing period, a chloride solution (3.3% NaCl), geothermal water – rich in sulphates –, and tap water as a reference. The exposures are labelled as XS, XA, and X0 respectively, coherently with Eurocode 2 and EN standards. The specimens were immersed in the exposures together with the bracing system. Numerous beams were tested, according to the scheme in Figure 2, to evaluate both the contribution of nanomaterials and the effect of aggressive exposures and their evolution over time. As shown in the figure, tests were performed at 1, 2, 3, 6, 9, and 12 months.

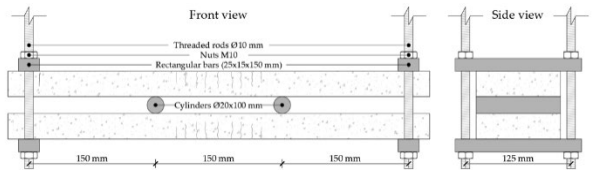

Figure 1. Schematics of the set-up to apply the sustained flexural loading while exposing the specimens to different conditions.

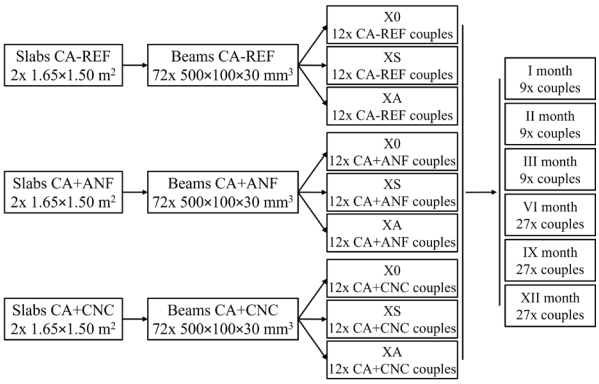

Figure 2. Layout of the experimental campaign.

The experimental campaign included multiple non-destructive and destructive tests, conducted at three different stages, according to the condition of the specimens; the first stage involved all the specimens in their virgin, uncracked condition. In the second stage, specimens were pre-cracked up to a prescribed level of damage, applied through 4-point bending tests, and measured in terms of total crack opening displacement (COD), which is the sum of the multiple cracks formed. The COD targeted at pre-cracking was 200 μm, measured with two horizontal LVDTs positioned at the bottom of the specimen. After unloading, residual crack

opening values ranged between 75 and 150 µm. Since all specimens were pre-cracked with 4-point bending scheme, numerous cracks formed in the central region of the beams. Only reference specimens at time 0 were not pre-cracked and not exposed. At the end of the second stage, the sustained loading was applied, bracing coupled beams (Figure 3). The specimens were then positioned inside tanks filled with three different solutions, namely chloride solution (3.3% NaCl concentration), geothermal water – rich in sulphates –, and tap water, used as reference. One couple of nominally identical specimens was provided for each scenario (i.e., exposure and time).

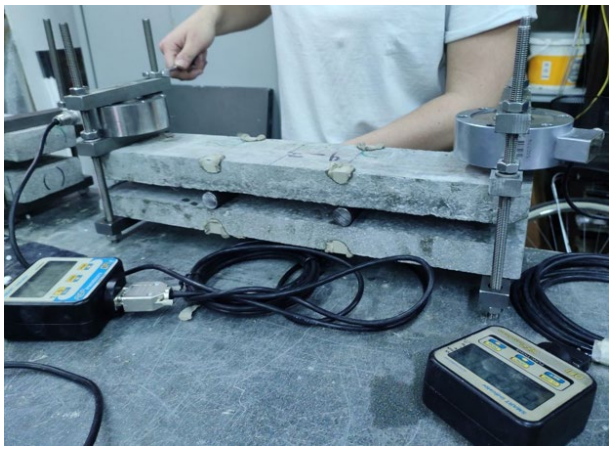

Figure 3. Application of the sustained loading employing the set-up shown in **Figure 1**.

After the exposure, the beam couplets were extracted to repeat the non-destructive measurements, and then they were tested both to failure, one under 4-point bending flexural test and the other with direct tensile test. A schematic representation of the tests conducted over the experimental campaign is provided in Table 2, where the tests considered for the present manuscript are highlighted.

Table 2. Stages of the experiments and tests performed.

Stage	Tests performed
Uncracked	Non-destructive: natural frequency of vibration, ultrasonic pulse velocity
Pre-cracked	Non-destructive: natural frequency of vibration, ultrasonic pulse velocity, crack width measurement
After exposure	Non-destructive: natural frequency of vibration, ultrasonic pulse velocity, crack width measurement **Destructive: 4-point bending/direct tension**

3.1 Direct tensile tests

Direct tensile tests were performed with a tailored setup, consisting of four steel plates placed at the ends of the specimen, on both sides (Figure 4). A specific bi-component glue was used to attach the plates to the beam, over a 140x100 mm^2 surface.

A crucial aspect related to the direct tensile test is the sensitivity of the test itself. Two factors mainly affected the values obtained from the tests. Firstly, the fibres tended to accumulate on the bottom of the mould, during the casting process. Thus, the distribution across the thickness was not homogeneous. This aspect was visible on the sides of the beams after cutting the casted slabs and in the cross-section after failure tests. The mechanical response observed during the tests further confirmed the hypothesis, since the first crack appeared on the weak side most of the times. Therefore, the response of the specimen was characterized by bending as well as direct tension. Furthermore, the sustained load applied to the beams, together with the pre-cracking process, resulted in a residual deflection, which worsened the aforesaid bending phenomenon.

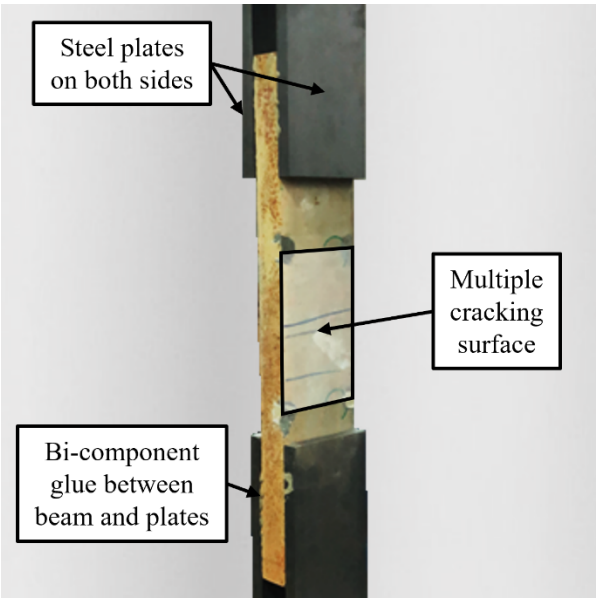

Figure 4. Setup of the direct tensile test.

3.2 Four-point bending and inverse analysis

For each specimen tested under direct tension, a nominally identical one was tested in 4-point bending. In order to identify the constitutive tensile response from the 4-point bending tests inverse analysis methods must be applied. The present work adapted a simplified methodology proposed by López et al. [18], which reproduces the typical strain-hardening response of materials such as UHPC through a quadrilinear constitutive law. The methodology is based on numerical correlations between five points in the σ_{fl}–δ curve (Figure 5a) obtained from 4-point bending test and five constitutive parameters used to obtain the constitutive law (Figure 5b). The law consists of two different bilinear parts: the first before the peak stress (i.e., ultimate tensile stress), which may include a strain hardening stage as induced by stable multiple cracking process, and the post-peak one, corresponding to the unstable localization and propagation of a single crack.

Since the methodology was calibrated in [18] for beams with length-to-thickness ratios either of 3.0 or 4.5, a normalized curve was derived to evaluate the differences with reference to the thin beams of the present experimental campaign, having L/h = 15. As shown in Figure 6, the slenderness has a remarkable

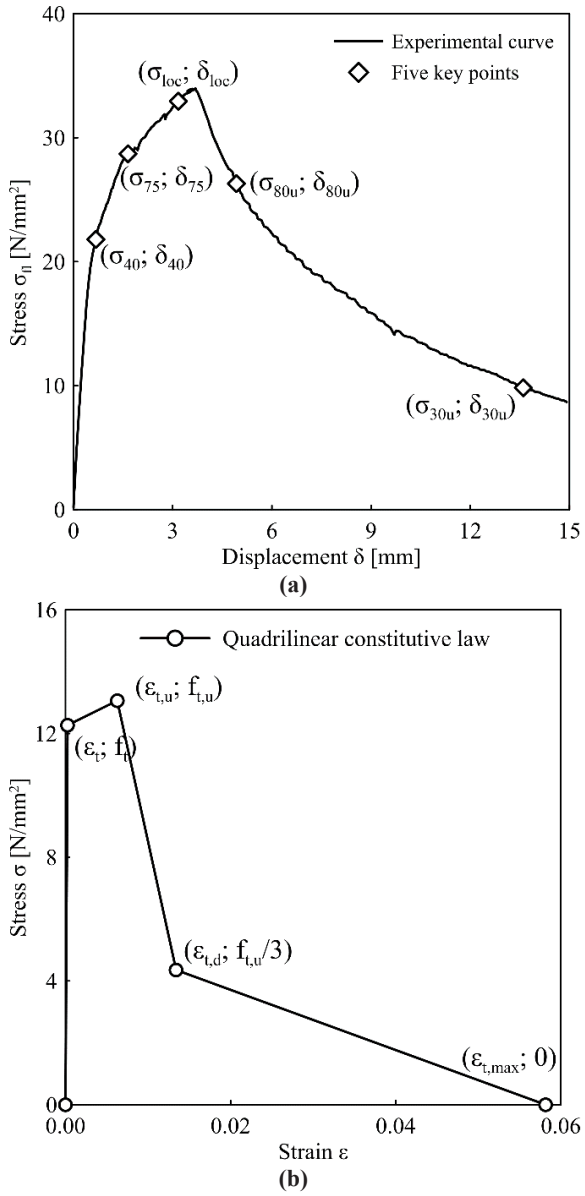

Figure 5. (a) Experimental curve with the five key points, and **(b)** quadrilinear constitutive law derived from the curve.

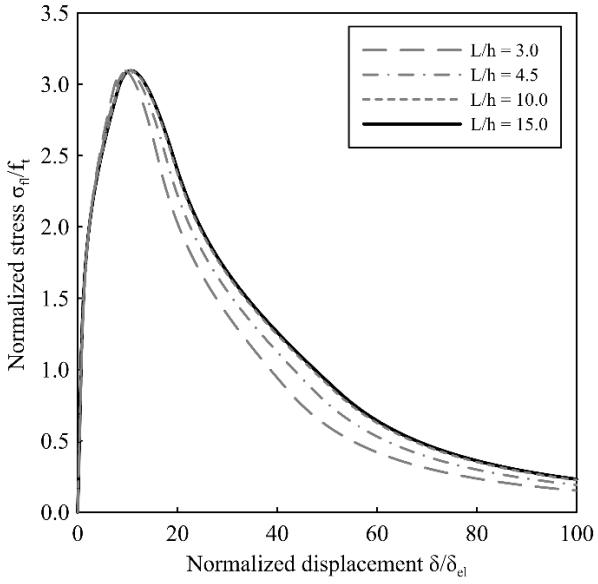

Figure 6. Effect of slenderness on numerical correlations.

effect on the results of the analysis. On the other side, for higher values of slenderness the difference is negligible. Hence, the variability of thickness among the specimens utilized for the experimental campaign could be disregarded. The procedure was repeated to determine the numerical relations between the key points of the σ_{fl}–δ curve and the constitutive parameters. After the Monte Carlo analysis, a fitting was operated to obtain the final form of the relations (Eq. 1-5).

$$f_t = \frac{\sigma_{75}}{1{,}64}\left(\frac{\sigma_{75}}{\sigma_{40}}\right)^{0{,}29} \quad (1)$$

$$\varepsilon_{t,u} = \frac{f_t}{E}\left(5{,}46\frac{\delta_{loc}}{\delta_{75}} - 1{,}70\right) \quad (2)$$

$$f_{t,u} = \alpha^{-0{,}21}\left(2{,}63\frac{\sigma_{loc}}{\sigma_{75}} - 1{,}90\right) f_t \quad (3)$$

$$\varepsilon_{t,d} = \gamma^{-0{,}45}\alpha^{1.06}\left(1{,}64\frac{\delta_{80u}}{\delta_{loc}} - 0{,}73\right)\frac{f_t}{E} \quad (4)$$

$$\varepsilon_{t,max} = 1{,}06\beta^{-0{,}64}\gamma^{-0{,}38}\alpha^{1.64}\left(\frac{\delta_{30u}}{\delta_{loc}}\right)^{1{,}84}\frac{f_t}{E} \quad (5)$$

4 Results

4.1 Direct tensile tests

The tensile response did not exhibit any significant variation among the three mixes, and the performance could be preserved over time (Figure 7a). After the first month of exposure, the damage induced by pre-cracking was not completely recovered. Hence, the tensile response was slightly lower on average. Self-healing mechanisms proved to be more effective at longer periods, showing a constant increase in the response from the third month to one year, when the results were comparable to the original performance.

The two mixes with nano-additions performed better at earlier ages, due to the contribution of alumina nano-fibres and cellulose nanocrystals. These respectively accelerated hydration and allowed to control cracks at smaller scale, preventing localization in the early phases and promoting multiple cracking [19–21].

The different exposures partially affected the recovery of the material (Figure 7b). During the first two months, the specimens exposed to geothermal water experienced a fast recovery of the mechanical performance, likely related to the precipitation of calcium, observed in chemical analyses of the geothermal water (203.4 mg/l after twelve months). A similar phenomenon was observed for chloride solution at two months. The chloride binding capacity of the cement might have fostered the sealing process [22]. Upon longer exposure periods, the differences among the environments are negligible, and only at twelve months a more pronounced recovery was observed for specimens in tap water. On average, in most cases, the specimens tested after exposure exhibited a poorer performance if compared to the reference ones. This is due to the pre-cracking and sustained loading, which compromised the straightness of the beams, resulting in

a combined effect of bending and direct tension which led to a premature failure.

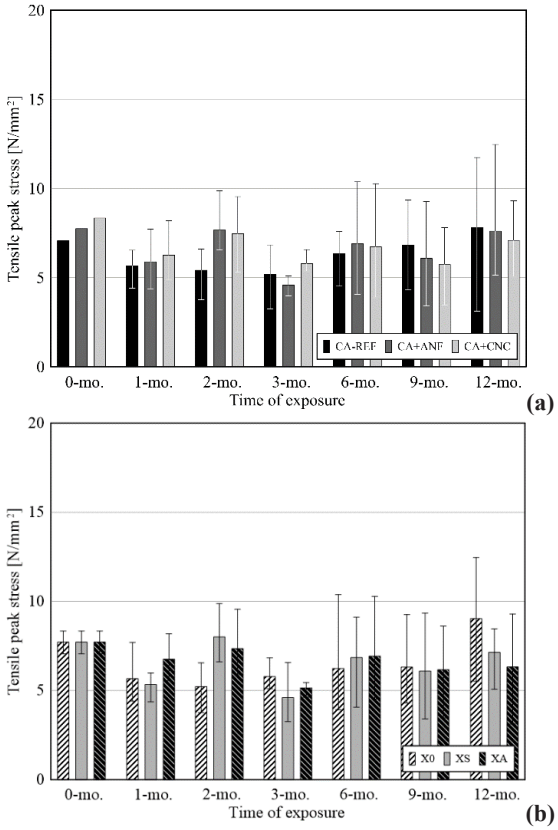

Figure 7. Tensile peak stress evolution over time **(a)** sorted by material, and **(b)** sorted by exposure.

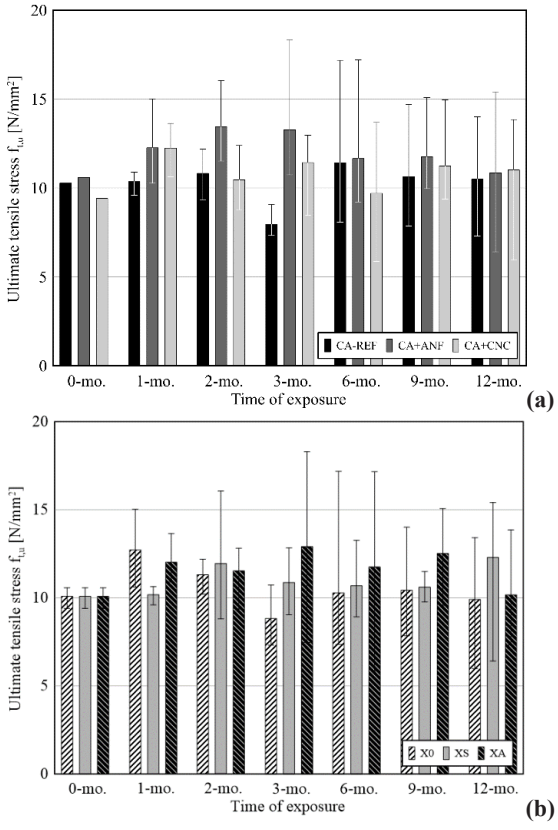

Figure 8. Ultimate tensile stress evolution over time **(a)** sorted by material, and **(b)** sorted by exposure.

4.2 Four-point bending tests and inverse analysis

The flexural tests confirmed the effects of alumina nano-fibres on the mechanical response of the beams (Figure 8a). In all the cases the stress values are higher than for the other two mixes. The recovery of the performance started since the earliest ages and was preserved over time. In 4-point bending test the tensile stress acts in the lower portion of the section, where most fibres are located. Hence, the inhomogeneity of the section had a limited effect on the mechanical performance, in opposition to the direct tensile tests, as commented above. Furthermore, the healing process enhanced the properties of the section, if compared to the virgin material, as described in [17]. The results of the inverse analysis did not exhibit any remarkable effect related to the exposure (Figure 8b). The average values remained approximatively constant over time, with a limited variability if compared to the scattering.

4.3 Comparison between the two methods

The purpose of the inverse analysis is to obtain the constitutive behaviour of the material from the results of 4-point bending test, which is easier to perform and more reliable than the direct tensile test. As already mentioned, the latter is susceptible to numerous factors, such as the homogeneity across the thickness of the specimen cross-section, the straightness of the specimen, and the same test setup. Therefore, direct tensile tests can be considered to provide a lower boundary of the actual response of the material. Figure 9 compares the peak tensile stress obtained from the direct test and the corresponding ultimate tensile stress $f_{t,u}$ obtained from inverse analysis of 4-.point bending test results of the nominally identical specimen.

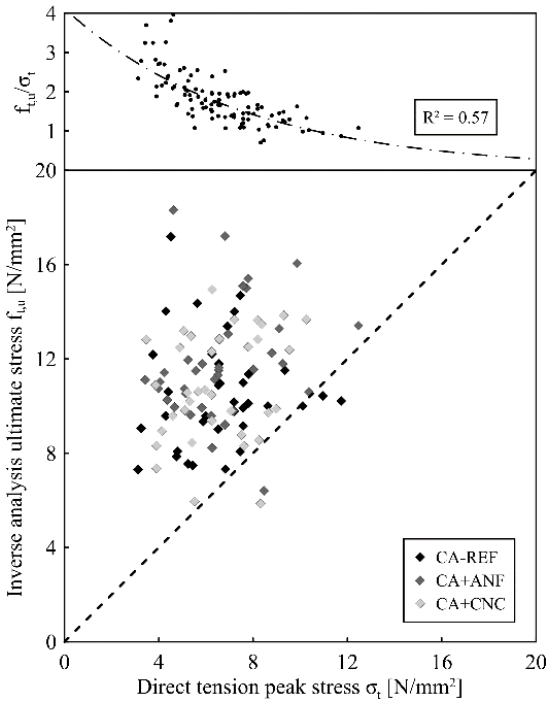

Figure 9. Comparison between direct tension and inverse analysis in terms of peak stress.

In most cases, the ultimate tensile stress obtained from inverse analysis is higher than the peak from direct tensile tests. The difference progressively reduces for higher values of direct tensile stress. The concentration of fibres on the bottom (i.e., tensile side) of the beam favoured the flexural response. Conversely, direct tensile tests were negatively affected by the uneven distribution of fibres in part of the cross-section, and, thus, lower stress values were obtained.

4.4 Evolution of the constitutive law

Self-healing proved to be effective to compensate the damage induced by pre-cracking and the accumulation of permanent deflection due to sustained loading. As a matter of fact, the specimens underwent real service life conditions, which for conventional concrete structures progressively affect the mechanical performance. Conversely, the autogenous healing capacity of UHPC resulted in the capacity of maintaining an approximatively constant tensile response over time. Since inverse analysis provided the complete stress-strain law from the 4-point bending tests, the evolution of the constitutive response was evaluated both in terms of elastic modulus and toughness. The former is a measure of the stiffness, which drives the mechanical response of the section for the elastic part. The latter includes the whole mechanical response of the section.

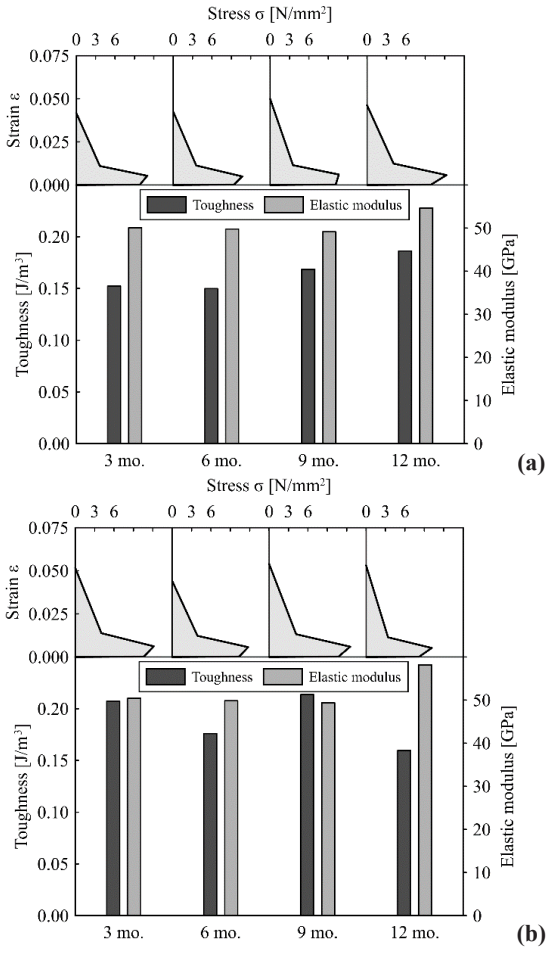

Figure 10. Evolution of the constitutive law over time for specimens in **(a)** chloride solution XS, and **(b)** geothermal water XA.

Figure 10 reports the evolution of the constitutive laws over time inside the two aggressive environments, together with the parameters previously introduced. The specimens immersed inside the chloride solution were able to preserve the elastic modulus over time, proving the effectiveness of the self-healing mechanism to counteract the negative effects of the applied load and the degradation that could occur. The contribution of self-healing is even more significant considering the toughness, which showed an increasing trend at longer periods, after the completion of crack sealing. Specimens exposed to geothermal water experienced a wider scattering in terms of toughness, related to the limited length of the softening branch at six months and to a possible degradation occurring after one year of exposure. Contrariwise, the elastic modulus was constant until nine months of exposure, and slightly increased after twelve months.

5 Conclusions

The present work has investigated the evolution of the tensile performance of a UHPC mix with enhanced self-healing capacity and different nano-additives (also denoted as Ultra High Durability Concrete UHDC). Thin beams were tested at different periods under real service life conditions – encompassing sustained flexural loading and aggressive exposure – to address the effects of the autogenous healing capability of the material through mechanical tests. Two different failure tests were performed, direct tension and 4-point bending. For the latter, a simplified inverse analysis was applied to extract the constitutive behaviour from a structural response.

According to the results discussed above, the following conclusions can be drawn.

- Direct tensile tests were strongly affected by the conditions of the specimen. Since the beams experienced pre-cracking and sustained flexural loadings, the resulting accumulated permanent long-term deflection, though limited, affected the test response. Moreover, the distribution of fibres caused the crack to form on the weak side, worsening the bending effect during the tests.
- Inverse analysis proved to be an effective method to obtain a constitutive response of UHPC. Since the method is based on a widely diffused testing methodology for fibre-reinforced concretes, it can be considered a suitable alternative to other tests like direct tension.
- Self-healing mechanisms counterbalanced the effects of the initial damage on the beams within a limited period. Additionally, autogenous healing allowed to preserve the mechanical performance of the material after longer periods, also resulting in a slight improvement in a few cases. The latter might be attributed to the chemical composition of the healing products and their interaction with the original material.
- Nano-additives promoted the early recovery of the induced damage, owing to the crack bridging capacity they provide at the nano-scale level.

- The three environments investigated did not result in remarkable differences among each other. The early performance recovery of the material, together with its high density, hindered the penetration of aggressive particles inside the matrix and limited the degradation of the specimens.

The research activity reported has been performed in the framework of the ReSHEALience project (Rethinking coastal defense and Green-energy Service infrastructures through enHancEd-durAbiLity high-performance cement-based materials) which has received funding from the European Union's Horizon 2020 research and innovation program under grant agreement No 760824. The information and views set out in this publication do not necessarily reflect the official opinion of the European Commission.
Francesco Soave acknowledges the support of MUSA – Multilayered Urban Sustainability Action–project, funded by the European Union –NextGenerationEU, under the National Recovery and Resilience Plan (NRRP) Mission 4 Component 2 Investment Line 1.5: Strengthening of research structures and creation of R&D "innovation ecosystems", set up of "territorial leaders" in R&D in funding the continuation of his studies through a Ph.D. scholarship.

References

1. A. Poonguzhali, H. Shaikh, R. Dayal, H. Khatak, Corrosion Reviews **26** (2008) 215-294.
2. M. Saeed Mirza, Can. J. Civ. Eng. **33** (2006) 650-672.
3. D. di Summa, J.R. Tenório Filho, D. Snoeck, P. van den Heede, S. van Vlierberghe, L. Ferrara, N. de Belie, J. Clean Prod. **358** (2022).
4. N.P. Kannikachalam, D. di Summa, R.P. Borg, E. Cuenca, M. Parpanesi, N. de Belie, L. Ferrara, ACI Mater. J. **120** (2023).
5. J.A. Mullard, M.G. Stewart, J. Bridge Eng. **17** (2012) 353-362.
6. R.D. Hooton, Cem. Concr. Res. **124** (2019) 1-17.
7. B.A. Graybeal, ACI Mater. J. **104** (2007) 146-152.
8. Z. Zhou, P. Qiao, J. Test. Eval. **48** (2018).
9. P. Serna, F. Lo Monte, E.J. Mezquida-Alcaraz, E. Cuenca, V. Mechtcherine, M. Reichardt, A. Peled, O. Regev, R.P. Borg, A. Tretjakov, D. Lizunov, K. Sobolev, S. Sideri, K. Nelson, E.M. Gastaldo Brac, L. Ferrara, (2019).
10. S. Al-Obaidi, P. Bamonte, L. Ferrara, M. Luchini, I. Mazzantini, Infrastructures (Basel) **5** (2020) 1-44.
11. S. Al Obaidi, P. Bamonte, F. Animato, F. Lo Monte, I. Mazzantini, M. Luchini, S. Scalari, L. Ferrara, Sustainability (Switzerland) **13** (2021) 1-26.
12. S. Al-Obaidi, M. Davolio, F. Lo Monte, F. Costanzi, M. Luchini, P. Bamonte, L. Ferrara, Case Studies in Constr. Mater. **17** (2022).
13. F. Lo Monte, L. Ferrara, Mater. and Struct./Mater. et Constr. **53** (2020) 1-12.
14. F. Lo Monte, L. Ferrara, Constr. Build. Mater. **283** (2021) 1-12.
15. A. de Souza Oliveira, O. da Fonseca Martins Gomes, L. Ferrara, E. de Moraes Rego Fairbairn, R.D. Toledo Filho, J. Build. Eng. **41** (2021).
16. E. Cuenca, M. Criado, M. Giménez, M.C. Alonso, L. Ferrara, J. Mat. Civ. Eng. **34** (2022) 1-17.
17. M. Davolio, S. Al-Obaidi, M.Y. Altomare, F. Lo Monte, L. Ferrara, Cem. Concr. Compos. (Submitted 30/12/2022).
18. J.Á. López, P. Serna, J. Navarro-Gregori, H. Coll, Compos. B Eng. **91** (2016) 189-204.
19. E. Cuenca, L. D'Ambrosio, D. Lizunov, A. Tretjakov, O. Volobujeva, L. Ferrara, Cem. Concr. Comp. **118** (2021) 1-17.
20. E. Cuenca, V. Postolachi, L. Ferrara, Constr. Build. Mater. (Submitted 25/09/2022).
21. E. Cuenca., A. Mezzena, L. Ferrara, Constr. Build. Mater. **266** (2021).
22. E. Cuenca, F. Lo Monte, M. Moro, A. Schiona, L. Ferrara, Sustainability (Switzerland) **13** (2021).